

Intramembrane Cavitation as a Predictive Bio-Piezoelectric Mechanism for Ultrasonic Brain Stimulation

Michael Plaksin, Shy Shoham^{*} and Eitan Kimmel[†]

Faculty of Biomedical Engineering & Russell Berrie Nanotechnology Institute,

Technion – Israel Institute of Technology, Haifa 32000, Israel

^{*},[†]Corresponding Authors Emails:

^{*} sshoham@bm.technion.ac.il.

[†] eitan@bm.technion.ac.il.

ABSTRACT. Low intensity ultrasonic waves can remotely and non-destructively excite central nervous system (CNS) neurons. While diverse applications for this effect are already emerging, the biophysical transduction mechanism underlying this excitation remains unclear. Recently, we suggested that ultrasound-induced intramembrane cavitation within the bilayer membrane could underlie the *biomechanics* of a range of observed acoustic bio-effects. Here, we show that in CNS neurons, ultrasound-induced cavitation of these nanometric bilayer sonophores can induce a complex mechano-electrical interplay leading to excitation, primarily through the effect of currents induced by membrane capacitance changes. Our model explains the basic features of CNS acousto-stimulation and predicts how the experimentally observed efficacy of mouse motor cortical ultrasonic stimulation depends on stimulation parameters. These results support the hypothesis that neuronal intramembrane piezoelectricity underlies ultrasound-induced neurostimulation, and suggest that other interactions between the nervous system and pressure waves or perturbations could be explained by this new mode of biological piezoelectric transduction.

Subject Areas: Biological Physics, Computational Physics, Acoustics.

I. INTRODUCTION

Ultrasound (US) is not only widely used for imaging [1]; its interaction with biological tissues is known to induce a wide variety of non-thermal effects ranging from hemorrhage and necrosis [2] to more delicate manipulations of cells and their membranes such as permeability enhancement [3], angiogenesis induction [4-6] and increased gene transfection [7]. In particular, both classical and recent studies have demonstrated that US can interact with the physiology of excitable tissues, inducing the generation of action potentials (APs) [8-16], suppression of nerve conduction [17-19] as well as more subtle changes in excitability [20-22]. While the suppression of nerve conduction is putatively dependent on temperature elevation [18,19], the biophysical basis of neural stimulation is not understood, and did not receive a rigorous, quantitative and predictive treatment. Recently, we introduced the bilayer sonophore (BLS) model as a unifying hypothesis for the underlying mechanism of multiple bio-acoustic interactions, wherein US preferentially induces intra-membrane cavitation or bubble formation in the intra-membrane space between the two lipid leaflets of the cell's membrane [23]. In the BLS model, the negative pressure phase of the US wave pulls the two leaflets away while the positive pressure pushes the leaflets towards each other; dissolved gas accumulates in the hydrophobic zone, creating pockets of gas that expand and contract periodically. BLS formation is predicted to induce various alterations in cells (bioeffects) including the initiation of cellular mechano-transduction processes, the induction of membrane pore formation and permeability changes. These bioeffects, which are naturally considered as associated with mechanical loading, were shown to systematically and predictably intensify as the US pressure amplitude increases or the frequency decreases, in softer tissues or close to free surfaces, and in the presence of microbubbles [23].

In an attempt to understand the mechanisms underlying the effect of US on excitable tissues, we analyze a Neuronal BLS (NBLS) framework where the bio-mechanics of intramembrane cavitation is coupled to membrane bio-electrical mechanisms in a complex interplay. This mechano-electrical coupling is shown to induce displacement currents that excite action potentials through an indirect mechanism, whose features explain the requirement for long ultrasonic stimulation pulses [12, 14, 16] and predict the experimentally observed efficacy of ultrasonic stimulation in mouse motor cortex [16].

II. MODEL & EQUATIONS

The purely mechanical BLS model was modified to account for the dynamics of membrane charge polarization, capacitance, and voltage-sensitive ion channels in a CNS neuron [*NBLS model* – Fig. 1(a)]. The NBLS model combines the modified BLS model and the Hodgkin-Huxley (H&H) model adapted for a regular spiking rat cortical pyramidal neuron [24]. Both BLS and H&H model parameters were taken "as is" without re-tuning or post-hoc adjustments, and are based on known or measured physical and biophysical quantities or ranges, wherever attainable (summarized in Table SI at Supplemental Material). The responses of the nanometer-scale BLS model to US are assumed to be representative of the responses of the whole cell; US waves with frequencies on the order of 1 MHz have wavelengths on the order of millimeters, orders of magnitude larger than the dimensions of CNS cortical neuron somata, so all BLS elements are subject to essentially the same acoustic effect. In the model, a circular, uniform phospholipid bilayer membrane patch is surrounded by a constraining circle of transmembrane proteins (64 nm diameter, based on average membrane inter-protein distances [25]). Electrically, the bilayer membrane has a

capacitance, and each ion has a Nernst equilibrium potential (V_{Na} , V_K , and V_{Leak}) and a time-dependent conductance, which generally depends on the product probabilities of multiple voltage-dependent gates [M and H gates for sodium channels and N and P gates for potassium channels, see Eq. (1)]. The deforming shape of the intra-membrane cavity [Fig. 1(b)] is driven by the time-dependent US pressure, leaflet tension, and an attraction-repulsion equivalent pressure resulting from phospholipids molecular forces and the electrostatic attraction forces between membrane charges [Fig. 1(c), top panels and Eq. (2)].

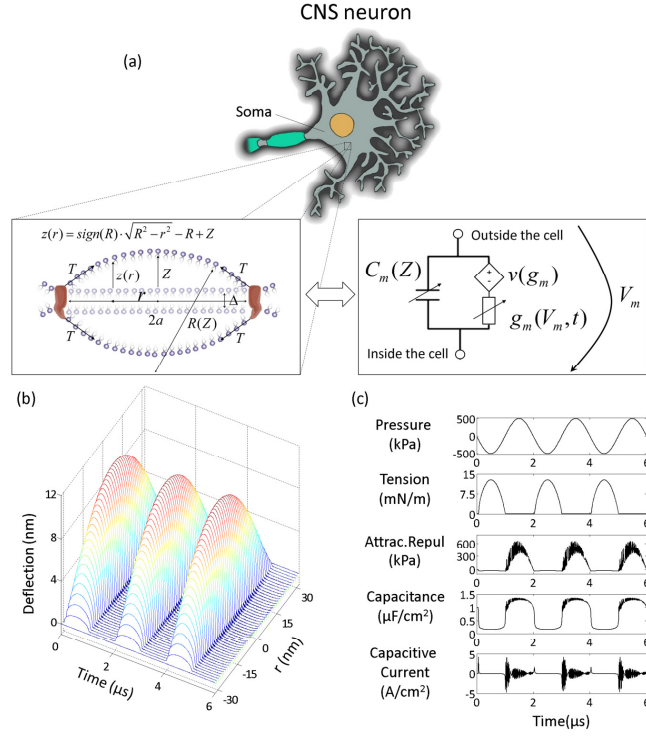


FIG. 1. Neuronal bilayer sonophore model. (a) Biomechanical and bioelectrical structure of NBLS model of small membrane patch in a CNS pyramidal neuron. A round patch of the bilayer leaflets (radius a , initial gap Δ) dynamically deforms into a dome shape with a maximal deflection Z , radius of curvature $R(Z)$ and tension T . The membrane equivalent circuit has a potential (V_m), time-varying capacitance (C_m), and Hodgkin-Huxley type ionic conductances (g_m) and sources [$v(g_m)$]. (b,c) Mechano-electrical dynamics of first three cycles of the model membrane exposed to US (pressure amplitude 500 kPa and frequency 0.5 MHz): (b) Local deflection at each radial coordinate [$z(r)$]. (c) Acoustic pressure (kPa), tension (mN/m), combined attraction/repulsion force per area between the leaflets (sum of molecular and electrostatic forces $P_M + P_{ec}$, kPa), membrane capacitance ($\mu F/cm^2$), and capacitive displacement current $\frac{dC_m}{dt} V_m$ (A/cm^2).

These dynamic deformations change the average membrane capacitance and induce a capacitive displacement current $\frac{dC_m}{dt}V_m$ [Fig. 1(c), bottom panels], which changes the membrane potential, thereby indirectly modulating the conductance of voltage-gated channels. The displacement current term is added to obtain a modified set of H&H equations for the open probabilities of voltage dependent sodium (m & h) and potassium (n & p) channels' gates:

$$\begin{aligned}
\frac{dV_m}{dt} &= -\frac{1}{C_m} \cdot \left[V_m \cdot \frac{dC_m}{dt} + G_{Na} \cdot (V_m - V_{Na}) + G_K \cdot (V_m - V_K) + G_M \cdot (V_m - V_K) + G_{Leak} \cdot (V_m - V_{Leak}) \right] \\
\dot{n}(t) &= \alpha_n \cdot (1-n) - \beta_n \cdot n \\
\dot{m}(t) &= \alpha_m \cdot (1-m) - \beta_m \cdot m \\
\dot{h}(t) &= \alpha_h \cdot (1-h) - \beta_h \cdot h \\
\dot{p}(t) &= (p_\infty - p) / \tau_p \\
G_{Na} &= \bar{G}_{Na} \cdot m^3 \cdot h \\
G_K &= \bar{G}_K \cdot n^4 \\
G_M &= \bar{G}_M \cdot p \\
G_{Leak} &= \bar{G}_{Leak} = const
\end{aligned} \tag{1}$$

where G_{Na} , G_K , G_M and G_{Leak} are the conductances of the sodium, delayed-rectifier potassium, slow non-inactivating potassium and the leak channels, respectively, and all voltage dependent parameters are defined in Ref. [24]. The time dependent C_m are associated with the geometrical shape of the deformed leaflets and can be determined by solving a modified dynamics force (pressure) balance equation that is based on the Rayleigh–Plesset (RP) equation for bubble dynamics [23,26]. The modified BLS equation,

$$\begin{aligned}
\frac{d^2Z}{dt^2} + \frac{3}{2R(Z)} \left(\frac{dZ}{dt} \right)^2 &= \\
\frac{1}{\rho_l |R(Z)|} \left[P_{in} + P_M + P_{ec} - P_0 + P_A \sin(\omega t) - P_s(Z) - \frac{4}{|R(Z)|} \cdot \frac{dZ}{dt} \left(\frac{3\delta_0 \mu_s}{|R(Z)|} + \mu_l \right) \right],
\end{aligned} \tag{2}$$

is the original force/pressure balance equation [23] with a new electric force/pressure term:

$$P_{ec} = -\frac{a^2}{Z^2 + a^2} \frac{(C_m \cdot V_m)^2}{2\epsilon_0\epsilon_r} \quad (3)$$

as well as slightly changed molecular forces between the phospholipid molecules in the opposite leaflets:

$$f(r) = A_r \left[\left(\frac{\Delta^*}{2z(r) + \Delta} \right)^m - \left(\frac{\Delta^*}{2z(r) + \Delta} \right)^n \right] \quad (4)$$

that are captured by an equivalent ‘molecular pressure’,

$$P_M = \frac{2}{Z^2 + a^2} \int_0^a f(r) r dr \quad (5)$$

where a , Z , $z(r)$ and $R(Z)$ are defined in Fig. 1; ρ_l is the membrane surrounding water-like medium density; ϵ_0 and ϵ_r are the dielectric and relative dielectric constants, respectively of vacuum and of the transmission medium between the two leaflets (ϵ_r chosen here to be equal to 1) and Δ and Δ^* are the initial gaps between the leaflets if there is or there is no charges on the membrane, respectively. Equation (3) accounts for the effective pressure due to the attraction forces between the electric ion charges on the membrane leaflets. The other pressure terms in Eq. (2) account for the surface tension [23] in the leaflets (P_s), and for the intra-membrane gas (air; N_2+O_2) pressure (P_{in}). The rest pressure is P_0 and the driving force/pressure is the US pressure pulse $P_A \sin(\omega t)$. The last pressure term on the RHS of Eq. (2) accounts for the viscous loss [23].

The value of P_{in} is determined by means of the following gas balance equation:

$$\begin{aligned}
\frac{dn_a}{dt} &= \frac{2 \cdot \pi (a^2 + Z^2) D_a}{\xi} \left[C_a - \frac{P_{in}}{k_a} \right], \\
n_a|_{t=0} &= \frac{P_0 \pi a^2 \Delta}{R_g T_{em}}, \\
P_{in} &= \frac{n_a R_g T_{em}}{V_a}
\end{aligned} \tag{6}$$

Equation (6) presents gas transport between two compartments: i) the dissolved gas compartment, with a uniform gas concentration (C_a) in the gas-saturated water, where D_a is the diffusion coefficient of the air in the water; and ii) the intra-membrane gaseous compartment, where k_a is the Henry coefficient, n_a is the mole content of ideal gas, R_g is the gas constant, T_{em} is the temperature and V_a is the intramembrane cavity volume which is expressed by:

$$V_a = \pi a^2 \Delta \left[1 + \frac{Z}{3\Delta} \left(\frac{Z^2}{a^2} + 3 \right) \right] \tag{7}$$

The gas transport takes place across a boundary layer with thickness ξ near the leaflet. For simplicity we assumed that $\xi = 0.5$ nm and as a result the gas reaches almost immediate equilibrium oscillations between the dissolved and the gaseous compartments. Such an assumption saves much time avoiding the complex calculations of the air concentration field in the surrounding medium, and is justified by the relative short times that required the intra-membrane space to reach stable oscillations [23]. We also assume that ($P_{in}(t=0) = P_0 = 10^5$ Pa) and that the initial gap between the leaflets is $\Delta = 1.26$ nm.

As the two leaflets of the BLS separate, deform and curve periodically with the US pressure, the membrane capacitance in Eqs. (1) and (3) is approximately derived by:

$$C_m(Z) = \frac{1}{\pi a^2} \int_0^{2\pi} \int_0^a \left(\frac{C_{m_0} \cdot \Delta}{2z(r) + \Delta} \right) r dr d\theta = \frac{C_{m_0} \cdot \Delta}{a^2} \left(Z + \frac{(a^2 - Z^2 - Z\Delta)}{2Z} \ln \left[\frac{2Z + \Delta}{\Delta} \right] \right) \tag{8}$$

which is based on a parallel plate capacitor expression per unit area and where the C_{m_0} is cell membrane capacity at rest.

III. RESULTS

A. Fundamental response to ultrasound and AP generation

We first studied the NBLS model's fundamental response to US stimulation. When continuous-wave (CW) US stimulates the model neuron, the intra-membrane space inflates and deflates at the US frequency [23], and the NBLS membrane potential oscillates strongly between -280 and -60 mV (Fig. 2, 0.35 MHz CW pulse, acoustic pressure amplitude 100 kPa, intensity 320 mW/cm² in a propagating wave). When the US stimulation stops after 30 ms a single AP will be generated after a short latency [Fig. 2(a)]. For increased US pulse duration [Fig. 2(b), 40 ms] the US stimulation leads to the generation of several APs *during* the stimulus (but starting at a later time). What is the detailed biophysical basis underlying AP generation in this model? Before the onset of US, the resting membrane potential is -72 mV, for which the voltage-dependent M, N and P gates are almost closed while the H gate is wide open. The US-induced oscillations are hyperpolarizing and further decrease the membrane potential [the transient periods of higher membrane potential are too short for the channels' response time constants: Fig. 2(a), bottom panels]. At this stage all voltage-dependent ion channels are closed, however, non-voltage-dependent ion channels remain open and fluctuating leak currents enter and exit the cell, causing a net elevation in the membrane's charge. When the US stimulation stops (after 30 ms), the membrane capacitance returns to its reference value, and the membrane potential is determined by the accumulated charge. The M gates will now be the first to respond to the membrane potential change - if it exceeds roughly -50 mV, a single AP is

rapidly generated [Fig. 2(a)]. When the pulse duration is increased [40ms, Fig. 2(b)], US stimulation leads to the generation of a few APs during the stimulus, primarily due to the gradual shift of the membrane potential oscillation range towards more depolarized values (e.g., from -280 to -60 mV at US onset and -160 to -35 mV, 33 ms later), gradually increasing the conductances of both sodium and potassium channels to relatively high values [Fig. 2(b), insets].

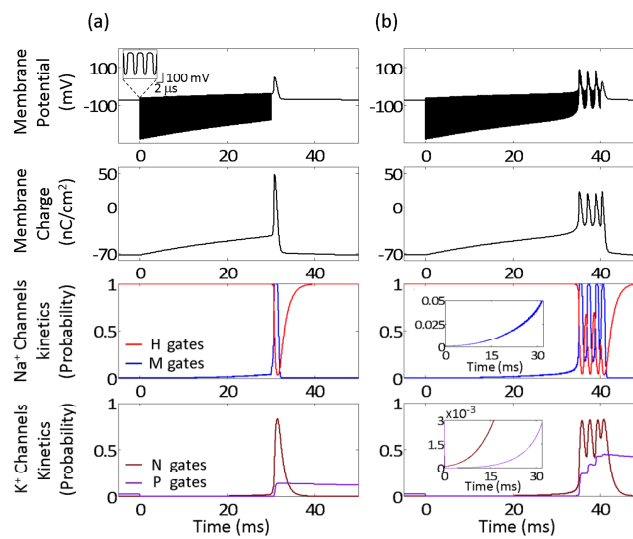


Fig. 2. The effect of continuous US stimuli (frequency 0.35 MHz , intensity 320 mW/cm²) on membrane potential & charge (top panels), and on sodium and potassium channels kinetics (bottom). (a) For stimulus duration of 30 ms, a single AP is generated immediately after the stimulus ends. Inset shows membrane potential oscillations. (b) For a stimulus duration of 40 ms, four APs are generated during the stimulus. Insets: magnified view of open probabilities for the M gate (Na⁺ channel kinetics) and the N and P gates (K⁺ channels).

This detailed mechanism is reminiscent of but very different from anodal break neuronal excitation [27]; US-induced excitation is not related to the inactivation state of the H channels, but is rather driven by the inability of channels to respond at the rates at which US-induced oscillations occur (in fact, anodal break does not occur in this particular neuron model [24]).

B. Dependence on ultrasound parameters

Next, we examined the influence of US frequency and duration on the threshold CW US intensity (and energy) required to generate an action potential and the number of APs generated. Intensity activation thresholds were found to monotonically (but weakly) increase with US frequency [Fig. 3(a)] and decrease with pulse duration at a fixed stimulation frequency [0.35 MHz, Fig. 3(b)], while threshold activation *energy* per unit area (intensity x duration) reaches a minimum at intermediate durations [~ 50 ms, Fig. 3(c)].

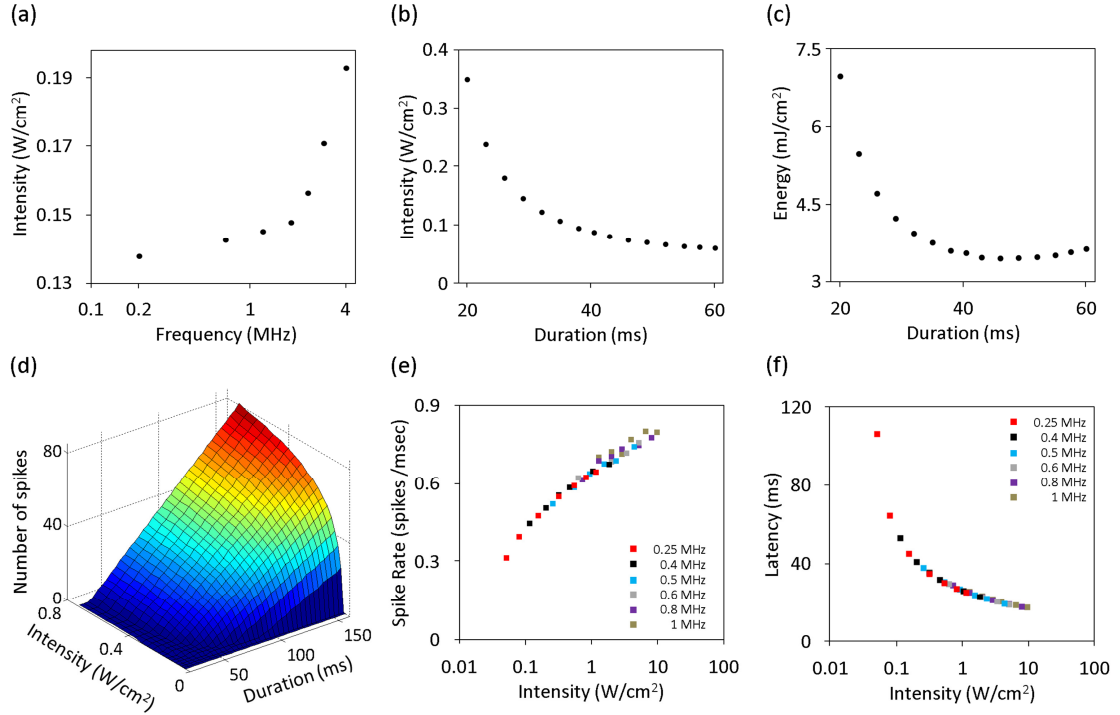


Fig. 3. Relationship between US stimulus parameters and APs generation in NBLs model. (a) Threshold intensity versus frequency required to generate a single AP (duration: 30 ms). (b,c) Threshold intensity and energy per unit membrane area versus stimulus duration required to generate a single AP (frequency: 0.35 MHz). (d) The number of APs induced by US stimuli as a function of US intensity and stimulus duration (frequency: 0.35 MHz). (e) Spike rate versus intensity for US frequencies (in MHz) of 0.25 (red squares), 0.4 (black squares), 0.5 (blue squares), 0.6 (gray squares), 0.8 (purple squares) and 1.0 (brown squares). (f) Latency before the appearance of the first AP during the US stimulation versus US intensity. Symbols and colors as in (e).

This frequency dependence is associated with increased inertia of the surrounding media against motion at higher frequencies, while the activation energy minimum is due to a tradeoff between charge accumulation and charge leakage as well as the relatively high molecular forces at low intensities.

Interestingly, excitation by direct injection of a short 1ms current pulse to the model neuron was found to require ~five orders of magnitude less intensity ($\sim 1.3 \mu\text{W}/\text{cm}^2$) and ~six orders of magnitude less energy ($\sim 1.3 \text{ nJ}/\text{cm}^2$) to elicit an action potential, highlighting the low energetic efficiency of the mechanical excitation process.

Above threshold, the number of APs generated increases monotonically with both intensity and duration [Fig. 3(d)]; as US intensity rises, the firing rate increases [Fig. 3(e)], while the latency to the first action potential decreases [Fig. 3(f)]. Both the rate and the latency are essentially frequency-independent at frequencies below 1 MHz [Fig. 3(e) and 3(f)]. This behavior can be explained by the relatively minor changes in threshold intensity for a single AP generation over the range of 0.2-4 MHz [Fig. 3(a)].

C. Biophysical model predicts *in vivo* results

Finally, to validate the NBLS model, we compared its predictions to the results of a recent *in vivo* study [16] where a wide range of US pulses were used to stimulate mouse primary motor cortex while resulting front limb muscle EMG signals were measured. To compare model predictions with experimental measurements we used Buckingham-Pi dimensional analysis [28] to relate NBLS' measures – the number of AP spikes (N), the response latency (L) and the overall duration of APs (D), to the experimental success rate (R_{sr}). Two dimensionless variables - N and the response “effectiveness” $D/(D+L)$ are associated with success rate in our model, but the latter quantity also appears to be solely a function of N (see Fig. S1 at Supplemental

Material). Therefore, R_{sr} depends only on N , a dependence that is well approximated by a sigmoidal-shaped logistic function (see the Appendix and Fig. S2 at Supplemental Material), and $R_{sr}(N)$ can be calibrated using this functional fit.

The calibrated *NBLS* model output was used to predict success rates for varying US frequencies and intensities under the conditions used by King *et al.* [16] : model predictions show an excellent qualitative agreement to their results [Fig. 4(a), stimulation pulses have 40,000 cycles and different frequencies].

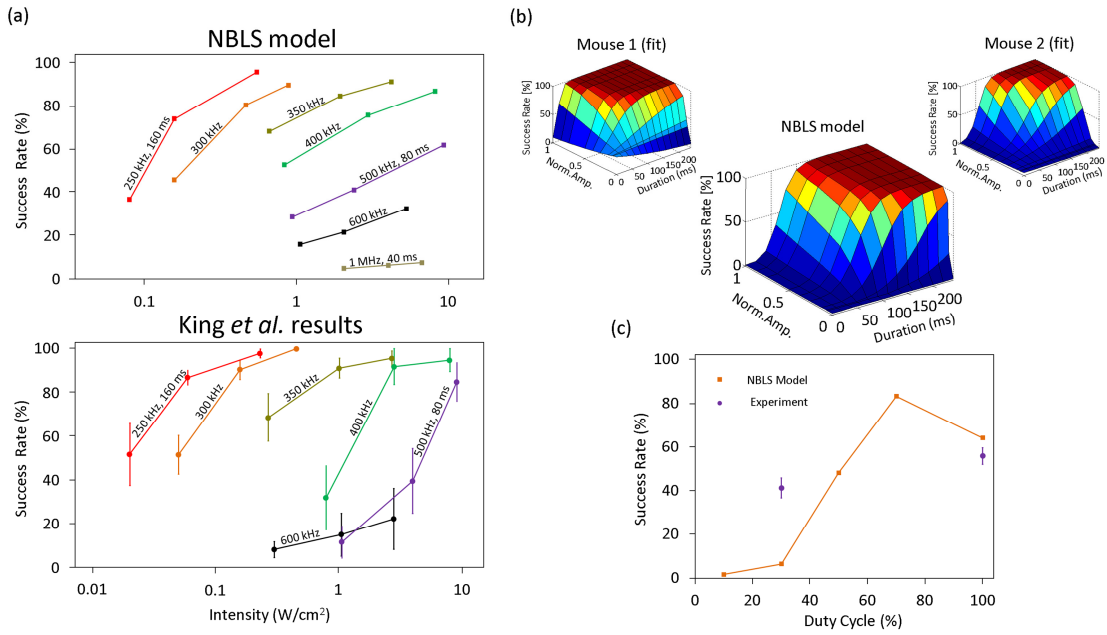


Fig. 4. Comparison of NBLS model predictions and *in-vivo* brain stimulation measurements [16]. (a) Success rates for eliciting motor responses versus US intensity at different frequencies (continuous stimulation for 40000 cycles). NBLS predictions (top panel) and the experimental results from Ref. [16] (bottom panel) are shown for US frequencies in the range 250 to 600 kHz (an additional 1 MHz simulation is also shown). Note that stimulus duration changes with the frequency (representative values shown). (b) Model-based predictions of success rate as a function of US pressure amplitude and stimulus duration (pressure amplitudes were normalized by maximal value used, 725 kPa; frequency: 0.5 MHz). For comparison, *in-vivo* measurements in two different mice [16] are shown in the upper part for the same US stimulation parameters. (c) Success rate as a function of duty cycle for simulation of NBLS model with pulsed-mode US (frequency: 0.5 MHz, Pulse repetition frequency: 1.5 kHz, stimulus duration: 80 ms, intensity: 10 W/cm² spatial peak pulse average). Two experimental data points from Ref. [16] are shown for duty cycle values 30 % and 100 % (stars, other US parameters were similar to the simulated values). Error bars represent the standard error of the mean.

Similar qualitative agreement is seen for 0.5 MHz US stimuli with varying pulse durations and pressure amplitudes (shown relative to the maximal used amplitude of 725 kPa or 16.8 W/cm²). For relatively short pulse durations and low US pressure amplitudes, a relatively low success rate is predicted [blue area in Fig. 4(b)]. When the pulse duration or the amplitude increases, the success rate increases gradually with power and duration until it reaches a plateau of 100 % success rates.

A final simulation study examined excitation by *pulsed* 0.5 MHz US for different intensities and duty cycle values (pulsed US is commonly used in applications which it is desirable to avoid heating the tissue, including neural stimulation). We found that the AP excitation mechanism for pulsed excitation was generally the same as for the CW mode (Fig. 2). Success probability for CW excitation was predictably higher than for 30 % duty cycle pulsed excitation, consistent with the experimental results [16]. Interestingly, however, a certain intermediate duty cycle value (~70 %) is predicted to have a maximal success rate, higher than for CW excitation [Fig. 4(c)].

IV. DISCUSSION

We studied a new biomechanical-biophysical mode of interaction between US and nerve cells with the goal of investigating the non-destructive manipulation of excitable tissues by US. Such an understanding can guide the development of future therapeutic applications of the only technology currently capable of *targeted non-invasive brain stimulation*. Exposing the NBLS element to simulated US results in rapid oscillatory hyperpolarizing currents and can lead to AP generation through a charge accumulation mechanism that results from the imbalance of ionic currents. This indirect, energetically inefficient excitation mechanism explains the characteristically very long pulses required for acousto-stimulation - tens to hundreds

of milliseconds [12, 14, 16], compared to sub-millisecond pulses typically used for electrical stimulation or even for photo-thermal stimulation [29, 30] (recently shown [31] to analogously be induced by *membrane capacitance changes* leading to depolarizing currents). Detailed model predictions were found to qualitatively agree with the results of recent *in-vivo* experiments in mice [16] (the first study where the effectiveness of a range of stimulation parameters was systematically examined). This agreement appears to support our underlying assumptions, simplifications and the natural choice of (unadjusted) parameters. In particular, it putatively supports using the response of a nanometric NBLS as predictive of the compound average behavior of the whole CNS neuron and of a whole neuronal population exposed to US (a realistic assumption given the millimeter-scale beam dimensions and wavelengths). It is also worth noting that intramembrane cavitation is not the only possible underlying mechanism for US-induced excitation; for example, the flexo-electricity model is a popular choice for explaining biological mechano-electrical conversion [32] and is also based on varying the curvature of the bilayer membrane. In Petrov's model the two membrane leaflets deform together as one sheet with roughly the same radius of curvature, while in our model the distance between the leaflets varies as they expand (and collapse) away from each other [Fig. 1(b)]. Our model is thus much more sensitive to acoustic pressure (acting *directly* to deform the BLS [23]) while deformations in the membrane's curvature from the negligible acoustic radiation pressures induced across the cell's membrane require unrealistic intensities for flexoelectric depolarizations of several millivolts.

The NBLS framework not only agrees with, but also sheds new light on experimental results. While the dependence of success rate on frequency [Fig. 4(a)] can be interpreted as strong [16], the model suggests that it is primarily a result of different

pulse durations used experimentally, while both number of APs and success rate are almost independent of the frequency [Figs. 3(e) and 3(f)]. It also predicts an optimal duty cycle for pulsed excitation [Fig. 4(c)], reflecting an optimal tradeoff between charge accumulation and M-gates ability to respond (preferentially during stimulus breaks). This result also highlights the potential of this model-based approach in the design of optimal acoustic excitation waveforms and strategies.

Finally, we speculate that this new mode of membrane-based US-induced piezoelectric transduction should exist in all polarized bilayer membranes, and it could be interesting to explore its properties, effects, and applications both in and out of the nervous system. Similar interactions to the ones we studied may underlie and/or shed new light on other types of biological mechano-electric coupling, from the sensation of sound vibration in the auditory system (where sub-Pascal scale threshold pressure amplitudes [33] could rely on hyper-sensitized NBLS-type mechanisms) and up to the impact of mega-Pascal pressure shocks that cause concussions and traumatic brain injury [34-36].

ACKNOWLEDGMENTS

We thank Roman Shusterman, Joshua Goldberg, Omer Naor, Steve Krupa and Amit Livneh for comments on the manuscript. This work was supported by the Russell Berrie Nanotechnology Institute, Johnson & Johnson Grant 1010051 and European Research Council Starting Grant 211055.

APPENDIX: MODEL SIMULATION AND VALIDATION DETAILS

The model's set of equations was numerically solved in Matlab (using the function ODE113). The time distance between the calculated points set to $0.025 / f \mu\text{s}$ (where f is the US frequency in MHz). The modified BLS model [Eqs. (2), (3), (4), (5), (6) and

(7)] was solved simultaneously with the H&H modified equations [Eqs. (1) and (8)] by updating the charge $C_m V_m$ in equation (3) every 500 μs . In each simulation run, the BLS model was solved as long as $Z(t)$ and $n_a(t)$ kept evolving in time. When both functions reached a stabilized periodic solution, we use Fourier series to incorporate it into Eq. (1).

For comparison between the theory and the experiments we introduced a logistic function,

$$R_{sr} = \frac{100}{1 + e^{\beta_0 + \beta_I N}} \quad (\text{A1})$$

where β_0 and β_I can be estimated from the *success rate* (R_{sr}) versus intensity (Table I at Ref. [16]), and the *number of AP spikes* (N) versus intensity predicted by NBLS model at US frequency of 0.5 MHz. Two data points were used (R_{sr} in percentage, N) (28.7, 34) and (52.9, 45). The calibration curve can be seen in Fig. S2 at Supplemental Material.

The intensity (I) in a propagating US CW [37] was calculated by:

$$I = \frac{P_A^2}{2\rho_l c} \quad (\text{A2})$$

where P_A is the pressure amplitude, ρ_l is the surrounding medium's density and c is the speed of sound in the medium. The spatial peak pulse average intensities in the pulsed mode simulations were calculated using Eq. (A2) as well.

REFERENCES

- [1] E. Macé, G. Montaldo, I. Cohen, M. Baulac, M. Fink, and M. Tanter, *Functional Ultrasound Imaging of the Brain*, Nat. Methods **8**, 662 (2011).
- [2] S.Z. Child, C.L. Hartman, L.A. Schery, and E.L. Carstensen, *Lung Damage from Exposure to Pulsed Ultrasound*, Ultrasound Med. Biol. **16**, 817 (1990).
- [3] S.M. Stieger, C.F. Caskey, R.H. Adamson, S. Qin, F.R. Curry, E.R. Wisner, and K.W. Ferrara, *Enhancement of Vascular Permeability with Low-Frequency Contrast-Enhanced Ultrasound in the Chorioallantoic Membrane Model*, Radiology **243**, 112 (2007).
- [4] S. Barzelai, O.S. Yosef, R. Holbova, D. Castel, R. Walden, S. Engelberg, and M. Scheinowitz, *Low-Intensity Ultrasound Induces Angiogenesis in Rat Hind-Limb Ischemia*, Ultrasound, Med. Biol. **32**, 139 (2006).
- [5] N. Mizrahi, D. Seliktar, and E. Kimmel, *Ultrasound-Induced Angiogenic Response in Endothelial Cells*, Ultrasound Med. Biol. **33**, 1818 (2007).
- [6] C.A. Johnson, S. Sarwate, R.J. Miller, and W.D. O'Brien, Jr., *A Temporal Study of Ultrasound Contrast Agent-Induced Changes in Capillary Density*, J. Ultrasound Med. **29**, 1267 (2010).
- [7] A. Lawrie, A.F. Briskin, S.E. Francis, D.I. Tayler, J. Chamberlain, D.C. Crossman, D.C. Cumberland, and C.M. Newman, *Ultrasound Enhances Reporter Gene Expression After Transfection of Vascular Cells In Vitro*, Circulation **99**, 2617 (1999).
- [8] E.N. Harvey, *The Effect of High Frequency Sound Waves on Heart Muscle and Other Irritable Tissues*, Am. J. Physiol. **91**, 284 (1929).
- [9] W.J. Fry, *Electrical Stimulation of Brain Localized without Probes: Theoretical Analysis of a Proposed Method*, J. Acoust. Soc. Am. **44**, 919 (1968).
- [10] L.R. Gavrilov, E.M. Tsurulnikov, and I.A. Davies, *Application of Focused Ultrasound for the Stimulation of Neural Structures*, Ultrasound Med. Biol. **22**, 179 (1996).
- [11] W.J. Tyler, Y. Tufail, M. Finsterwald, M.L. Tauchmann, E.J. Olson, and C. Majestic, *Remote Excitation of Neuronal Circuits Using Low-Intensity, Low-Frequency Ultrasound*, PLoS ONE **3**, e3511 (2008).
- [12] Y. Tufail, A. Matyushov, N. Baldwin, M.L. Tauchmann, J. Georges, A. Yoshihiro, S.I. Tillery, and W.J. Tyler, *Transcranial Pulsed Ultrasound Stimulates Intact Brain Circuits*, Neuron **66**, 681 (2010).
- [13] O. Naor, Y. Hertzberg, E. Zemel, E. Kimmel, and S. Shoham, *Towards Multifocal Ultrasonic Neural Stimulation II: Design Considerations for an Acoustic Retinal Prosthesis*, J. Neural. Eng. **9**, 026006 (2012).
- [14] H. Kim, S.J. Taghados, K. Fischer, L.S. Maeng, S. Park, and S.S. Yoo, *Noninvasive Transcranial Stimulation of Rat Abducens Nerve by Focused Ultrasound*, Ultrasound Med. Biol. **38**, 1568 (2012).
- [15] M.D. Menz, O. Oralkan, P.T. Khuri-Yakub, and S.A. Baccus, *Precise Neural Stimulation in the Retina Using Focused Ultrasound*, J. Neurosci. **33**, 4550 (2013).
- [16] R.L. King, J.R. Brown, W.T. Newsome, and K.B. Pauly, *Effective Parameters for Ultrasound-Induced In Vivo Neurostimulation*, Ultrasound Med. Biol. **39**, 312 (2013).

- [17] R.R. Young, and E. Henneman, *Functional Effects of Focused Ultrasound on Mammalian Nerves*, Science **134**, 1521 (1961).
- [18] P.P. Lele, *Effects of Focused Ultrasonic Radiation on Peripheral Nerve, with Observations on Local Heating*, Exp. Neurol. **8**, 47 (1963).
- [19] V. Colucci, G. Strichartz, F. Jolesz, N. Vykhodtseva, and K. Hynynen, *Focused Ultrasound Effects on Nerve Action Potential In Vitro*, Ultrasound Med. Biol. **35**, 1737 (2009).
- [20] J.S. Halle, C.R. Scoville, and D.G. Greathouse, *Ultrasound's Effect on the Conduction Latency of the Superficial Radial Nerve in Man*, Phys. Ther. **61**, 345 (1981).
- [21] J.H. Moore, J.H. Gieck, E.N. Saliba, D.H. Perrin, D.W. Ball, and F.C. McCue, *The Biophysical Effects of Ultrasound on Median Nerve Distal Latencies*, Electromyogr. Clin. Neurophysiol. **40**, 169 (2000).
- [22] P.H. Tsui, S.H. Wang, and C.C. Huang, *In Vitro Effects of Ultrasound with Different Energies on the Conduction Properties of Neural Tissue*, Ultrasonics **43**, 560 (2005).
- [23] B. Krasovitski, V. Frenkel, S. Shoham, and E. Kimmel, *Intramembrane Cavitation as a Unifying Mechanism for Ultrasound-Induced Bioeffects*, Proc. Natl. Acad. Sci. U. S. A. **108**, 3258 (2011).
- [24] M. Pospischil, M.T. Rodriguez, C. Monier, Z. Piwkowska, T. Bal, Y. Frégnac, H. Markram, and A. Destexhe, *Minimal Hodgkin–Huxley Type Models for Different Classes of Cortical and Thalamic Neurons*, Biol. Cybern. **99**, 427 (2008).
- [25] A. Pralle, *Physical Properties of the Plasma Membrane Studied by Local Probe Techniques* (Munich University Dissertations, Munich, Germany, 1998).
- [26] J. Wu, and W.L. Nyborg, *Ultrasound, Cavitation Bubbles and their Interaction with Cells*, Adv. Drug Deliv. Rev. **60**, 1103 (2008).
- [27] R. Guttman, and L. Hachmeister, *Anode Break Excitation in Space-Clamped Squid Axons*, Biophys. J. **12**, 552 (1972).
- [28] E. Buckingham, *On Physically Similar Systems: Illustrations of the Use of Dimensional Equations*, Phys. Rev. **4**, 345 (1914).
- [29] N. Farah, I. Brosh, C.R. Butson, and S. Shoham, *Photo-Thermal Neural Excitation by Extrinsic and Intrinsic Absorbers: a Temperature-Rate Model*, arXiv:1201.4617.
- [30] N. Farah, A. Zoubi, S. Matar, L. Golan, A. Marom, I. Brosh, and S. Shoham, *Holographically Patterned Activation Using Photo-Absorber Induced Neural Thermal Stimulation (PAINTS)*, J. Neural Eng. In press
- [31] M.G. Shapiro, K. Homma, S. Villarreal, C.P. Richter, and F. Bezanilla, *Infrared Light Excites Cells by Changing Their Electrical Capacitance*, Nat. Commun. **3**, 736 (2012).
- [32] A.G. Petrov, *Flexoelectricity of Model and Living Membranes*, Biochim. Biophys. Acta. **1561**, 1 (2002).
- [33] S. A. Gelfand, *Hearing: an Introduction to Psychological and Physiological Acoustics* (Informa Healthcare, Chippenham, England, 2009), 5th ed.

- [34] D. W. Brands, G. W. Peters, and P. H. Bovendeerd, *Design and Numerical Implementation of a 3-d Non-Linear Viscoelastic Constitutive Model for Brain Tissue During Impact*, J. Biomech. **37**, 127 (2004).
- [35] P.A. Taylor, and C.C. Ford, *Simulation of Blast-Induced Early Time Intracranial Wave Physics Leading to Traumatic Brain Injury*, J. Biomech. Eng. **131**, 061007 (2009).
- [36] M.K. Nyein, A.M. Jason, L. Yu, C.M. Pita, J.D. Joannopoulos, D.F. Moore, and R.A. Radovitzky, *In Silico Investigation of Intracranial Blast Mitigation with Relevance to Military Traumatic Brain Injury*, Proc. Natl. Acad. Sci. U. S. A. **107**, 20703 (2010).
- [37] W.R. Hendee, and E.R. Ritenour, *Medical Imaging Physics* (John Wiley & Sons, New York, 2002), 4th ed.

Intramembrane cavitation as a predictive bio-piezoelectric mechanism for ultrasonic brain stimulation

Supplemental Material

Michael Plaksin, Shy Shoham^{*} and Eitan Kimmel[†]

Faculty of Biomedical Engineering & Russell Berrie Nanotechnology Institute,

Technion – Israel Institute of Technology, Haifa, Israel 32000

Table SI. Parameters for the simulation runs of the NBLS model.

Parameter	Symbol	Unit	Value	Source
Thickness of the leaflet.	δ_0	nm	2	[S1]
Initial gap between the two leaflets if there is no charge on the membrane.	Δ^*	nm	1.4	[S2]
Initial gap between the two leaflets if there is charge on the membrane.	Δ	nm	1.26	Calculated from equilibrium state
Attraction/repulsion pressure coefficient.	A_r	Pa	10^5	[S2]
Exponent in the repulsion term.	m	-	5	
Exponent in the attraction term.	n	-	3.3	
Dynamic viscosity of the leaflets.	μ_s	Pa·s	0.035	Educated guess
Dynamic viscosity of the surrounding medium.	μ_l	Pa·s	$0.7 \cdot 10^{-3}$	[S3]
Diffusion coefficient of air in the surrounding medium.	D_a	$\text{m}^2 \cdot \text{s}^{-1}$	$3 \cdot 10^{-9}$	[S4]
Density of the surrounding medium.	ρ_l	$\text{kg} \cdot \text{m}^{-3}$	1028	[S5]
Speed of sound in the surrounding medium.	c	$\text{m} \cdot \text{s}^{-1}$	1515	
Initial air molar concentration in the surrounding medium ($\text{O}_2 + \text{N}_2$).	C_a	$\text{mol} \cdot \text{m}^{-3}$	0.62	[S3, S6, S7]
Henry's constant for dissolved air in the surrounding medium.	k_a	$\text{Pa} \cdot \text{m}^3 \cdot \text{mol}^{-1}$	$1.63 \cdot 10^5$	
Static pressure in the surrounding medium.	P_0	Pa	10^5	

Parameter	Symbol	Unit	Value	Source
The radius of the leaflet's boundary.	a	nm	32	Selection based on [S8]
The boundary layer length between the surrounding medium and the leaflets.	ξ	nm	0.5	Educated guess
The areal modulus of the bilayer membrane.	k_s	$\text{N}\cdot\text{m}^{-1}$	0.24	Selection based on [S9]
Surrounding medium's temperature.	Tem	K	309.15	[S10]
The maximal conductance of the Na^+ channels.	\bar{G}_{Na}	$\text{mS}\cdot\text{cm}^{-2}$	56	
The maximal conductance of the K^+ channels.	\bar{G}_K	$\text{mS}\cdot\text{cm}^{-2}$	6	
The maximal conductance of the slow K^+ channels.	\bar{G}_M	$\text{mS}\cdot\text{cm}^{-2}$	0.075	
The maximal conductance of the non-voltage-dependent ion channels.	\bar{G}_{Leak}	$\text{mS}\cdot\text{cm}^{-2}$	0.0205	
The Nernst potential of the Na^+ channels.	V_{Na}	mV	50	
The Nernst potential of the K^+ channels.	V_K	mV	-90	
The Nernst potential of the non-voltage-dependent ion channels.	V_{Leak}	mV	-70.3	
Spike threshold adjustment parameter.	V_T	mV	-56.2	
The decay time constant for adaptation at slow potassium channels.	τ_{\max}	ms	608	
The cell membrane capacity at rest.	C_{m_0}	$\mu\text{F}\cdot\text{cm}^{-2}$	1	
The rest potential of the cell membrane.	V_{m_0}	mV	-71.9	
Relative permittivity of the intramembrane cavity.	ε_r	-	1	Educated guess
Logistic function parameter.	β_0	-	4.08	Calculated from [S5]
Logistic function parameter.	β_1	-	-0.093	

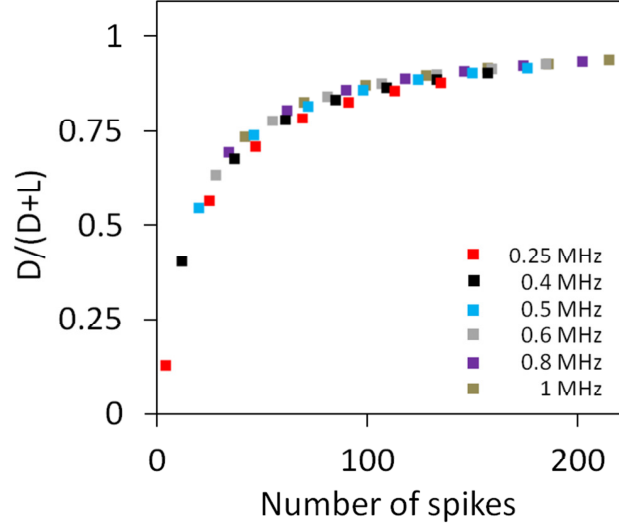


Fig. S1. The NBLS response "effectiveness" curve. Simulation results for $D/(L+D)$ as a function of the number of spikes for US frequencies of 0.25, 0.4, 0.5, 0.6, 0.8 and 1 MHz. One can observe the weak dependence on US frequency.

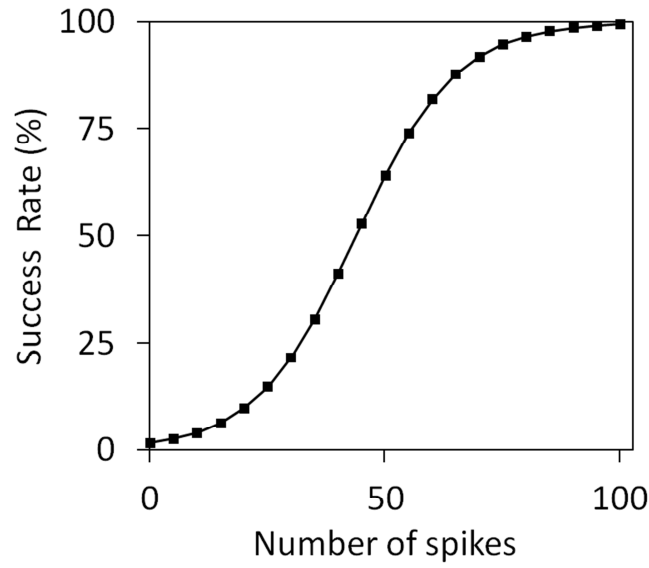


Fig. S2. Calibration curve between the NBLS model and the experimental results [S5]. Calibration curve of R_{sr} vs. N , where R_{sr} is the success rate and N is the number of spikes.

REFERENCES FOR SUPPLEMENTAL MATERIAL

- [S1] D. Boal, *Mechanics of the Cell* (Cambridge University Press, Cambridge, England, 2002).
- [S2] J.N. Israelachvili, *Intermolecular and Surface Forces* (Academic Press, London, England, 1992), 2nd ed.
- [S3] H.Y. Wong, *Handbook of Essential Formulae and Data on Heat Transfer for Engineers* (Longman, London, England, 1977).
- [S4] D.L. Wise, and G. Houghton, *The Diffusion Coefficients of Ten Slightly Soluble Gases in Water at 10-60 °C*, Chem. Eng. Sci. **21**, 999 (1966).
- [S5] R.L. King, J.R. Brown, W.T. Newsome, and K.B. Pauly, *Effective Parameters for US-Induced In Vivo Neurostimulation*, Ultrasound Med. Biol. **39**, 312 (2013).
- [S6] R. Sun, W. Hu, and Z. Duan, *Prediction of Nitrogen Solubility in Pure Water and Aqueous NaCl Solutions up to High Temperature, Pressure, and Ionic Strength*, J. Solution Chem. **30**, 561 (2001).
- [S7] M. Geng, and Z. Duan, *Prediction of Oxygen Solubility in Pure Water and Brines up to High Temperatures and Pressures*, Geochim. Cosmochim. Ac. **74**, 5631 (2010).
- [S8] A. Pralle, *Physical Properties of the Plasma Membrane Studied by Local Probe Techniques* (Munich University Dissertations, Munich, Germany, 1998)
- [S9] R. Phillips, T. Ursell, P. Wiggins, and P. Sens, *Emerging Roles for Lipids in Shaping Membrane-Protein Function*, Nature **459**, 379 (2009).
- [S10] M. Pospischil, M.T. Rodriguez, C. Monier, Z. Piwkowska, T. Bal, Y. Frégnac, H. Markram, and A. Destexhe, *Minimal Hodgkin–Huxley Type Models for Different Classes of Cortical and Thalamic Neurons*, Biol. Cybern. **99**, 427 (2008).